Terahertz Channel Model and Link Budget Analysis for Intrabody Nanoscale Communication

Hadeel Elayan, *Student Member, IEEE*, Raed M. Shubair, *Senior Member, IEEE*, Josep Miquel Jornet, *Member, IEEE*, and Pedram Johari, *Member, IEEE*

Abstract—**Nanosized devices operating inside the human body open up new prospects in the healthcare domain. *Invivo* wireless nanosensor networks (iWNSNs) will result in a plethora of applications ranging from intrabody health-monitoring to drug-delivery systems. With the development of miniature plasmonic signal sources, antennas, and detectors, wireless communications among intrabody nanodevices will expectedly be enabled at both the terahertz band (0.1–10 THz) as well as optical frequencies (400–750 THz). This result motivates the analysis of the phenomena affecting the propagation of electromagnetic signals inside the human body. In this paper, a rigorous channel model for intrabody communication in iWNSNs is developed. The total path loss is computed by taking into account the combined effect of the spreading of the propagating wave, molecular absorption from human tissues, as well as scattering from both small and large body particles. The analytical results are validated by means of electromagnetic wave propagation simulations. Moreover, this paper provides the first framework necessitated for conducting link budget analysis between nanodevices operating within the human body. This analysis is performed by taking into account the transmitter power, medium path loss, and receiver sensitivity, where both the THz and photonic devices are considered. The overall attenuation model of intrabody THz and optical frequency propagation facilitates the accurate design and practical deployment of iWNSNs.**

Index Terms—**Terahertz, intrabody channel model, wireless nanosensor networks, link budget, photonic.**

I. INTRODUCTION

THE engineering community is witnessing a new frontier in the communication industry. Among others, the tools provided by nanotechnologies enable the development of novel nanosensors and nanomachines. On the one hand, nanosensors are capable of detecting events with unprecedented accuracy. On the other hand, nanomachines are envisioned to accomplish tasks ranging from computing and data storing to sensing and actuation [1]. Recently, in vivo wireless nanosensor networks (iWNSNs) have been presented to provide fast and accurate disease diagnosis and treatment. These networks are capable of operating inside the human body in real time and will be of great benefit for medical monitoring and medical implant communication [2].

Despite the fact that nanodevice technology has been witnessing great advancements, enabling the commuication among nanomachines is still a major challenge. Classical communication paradigms need to undergo a profound revision before being used in nanonetworks. One of the mechanisms being comprehensively investigated is molecular communication [3], which is based on the exchange of molecules to transmit information. However, there are still many fundamental challenges to address, including the development of mechanisms to overcome the very long latency in molecular systems or the potential interference with biological molecular processes. Ultrasonic communication, based on the use of very high frequency acoustic signals, has also been recently proposed [4]. Nonetheless, for the time being, the size and power limitations of ultrasonic acoustic transducers pose a major challenge in their integration with biological nanosensors.

From the electromagnetic (EM) perspective, the miniaturization of a conventional metallic antenna to meet the size requirements of a nanosensor results in very high resonant frequencies, in the order of several hundreds of terahertz (THz or 10^{12} Hz). Accordingly, novel plasmonics have been recently proposed for wireless communication among nanodevices [5], [6]. These nanoantennas enable the wireless interconnection amongst nanosensors deployed inside and over the human body resulting in many bio-nanosensing applications [7]. For the time being, several works exist pointing to both the Terahertz Band (0.1-10 THz) as well as the infrared and optical transmission windows [8], [9]. While the majority of (nano) biosensing applications rely on the use of light, the propagation of THz signals within the human body remain largely unknown.

While the THz-band radiation is non-ionizing, the propagation of THz-band waves inside the human body is drastically impacted by the absorption of liquid water molecules [10]. As a result, Guo *et al*. [11], advocated the use of the

H. Elayan is with the Department of Electrical and Computer Engineering, Khalifa University, Abu Dhabi 127788, UAE (e-mail: hadeel.mohammad@kustar.ac.ae).

R. M. Shubair is with the Department of Electrical and Computer Engineering, Khalifa University, Abu Dhabi, UAE, and also with the Research Laboratory of Electronics, Massachusetts Institute of Technology, Cambridge, MA 02139 USA (e-mail: rshubair@mit.edu).

J. M. Jornet and P. Johari are with the Department of Electrical Engineering, University at Buffalo, the State University of New York, Buffalo, NY 14260 USA (e-mail: jmjornet@buffalo.edu; pedramjo@buffalo.edu).

optical window for intrabody wireless communication among nanosensors with plasmonic nanoantennas. This is due to the fact that the absorption from liquid water molecules is minimal in the so-called optical window, roughly between 400 THz and 750 THz [12]. In addition, plasmonic nanodevices at optical frequencies have already been utilized in several in vivo applications [13].

In this paper, a novel channel model for intrabody communication in iWNSNs in the THz band as well as optical window is presented. In particular, a mathematical framework is developed to compute the path loss by taking into account the spreading of the propagating wave, absorption from different types of molecules, as well as scattering of both the cells and the medium background. The results provided illustrate the design principles of iWNSNs. This paper also provides the first framework in the literature for conducting link budget analysis between nanodevices operating within the human body. This analysis is performed by taking into account the transmitter power, medium path loss and receiver sensitivity. Based on the application and distance of operation between nano-sensors, the user can select either the THz or optical frequencies.

The rest of the paper is organized as follows. In Sec. II, we discuss intrabody wave propagation losses considering the effect of spreading, molecular absorption as well as scattering. In Sec. III, THz and photonic technologies utilized in communications are presented to provide an insight on the link budget required for nanoscale intrabody communication. In Sec. IV, the numerical results are illustrated where the absorption and scattering coefficients are calculated and the total path loss at the THz and optical frequency is computed. Finally, we draw our conclusions in Sec. V.

II. Intrabody Wave Propagation Losses

The total path loss at both the THz and optical frequencies is contributed by three frequency-dependent terms: the spreading loss factor $L_{spr}(f)$, the molecular absorption loss factor $L_{abs}(f)$ and the scattering loss factor $L_{sca}(f)$. Each of these terms represents the ratio of the output to input powers for a particular intrabody distance. More specifically, the total attenuation factor is given by

$$L_{tot}(f) = L_{spr}(f) \times L_{abs}(f) \times L_{sca}(f). \quad (1)$$

The analytical model which will be presented in this paper focuses on the frequencies between 0.1-10 THz or, equivalently, wavelengths between 30 micrometers and 3 millimeters as well as frequencies between 400-750 THz, which correspond to wavelengths between 400 nanometer and 750 nanometer. Moreover, since the THz band lies in the middle ground between microwaves/millimeter waves and infrared, both frequency (f) and wavelength (λ) are common notations.

A. Intrabody Path Loss Due to Wave Spreading in Human Tissue

EM waves suffer from the spreading of energy, which is quantitatively described in the case of spherical propagation by the well-known inverse-squared distance function

$$L_{spr} = D\left(\frac{\lambda_g}{4\pi d}\right)^2, \quad (2)$$

where λ_g, the effective wavelength, is λ/n', n' and n'' are the real and imaginary parts of the tissue refractive index n, respectively. The tissue refractive index n is given by

$$n = n' - jn''. \quad (3)$$

It is worth noting that $n = \sqrt{\epsilon_r}$, where ϵ_r is the relative permittivity. The relative permeability is accounted as $\mu_r = 1$, since the biological tissues show almost no magnetic behavior [14], [15].

The directivity, D, refers to the maximum gain of the nanoantenna, and is given by the ratio of the maximum power density $P(\theta, \phi)_{max}$ in W/m^2 to its average value over a sphere, as observed in the far field of an antenna. Thus,

$$D = \frac{P(\theta, \phi)_{max}}{P(\theta, \phi)_{av}}. \quad (4)$$

From [16], the final form of the directivity is given by

$$D = \frac{4\pi}{\iint_{4\pi} P_n(\theta, \phi) d\Omega} = \frac{4\pi}{\Omega_A}, \quad (5)$$

where $P_n(\theta, \phi) d\Omega = P(\theta, \phi)/P(\theta, \phi)_{max}$ is the normalized power pattern, and Ω_A refers to the radiation solid angle. This angle depends on the specific radiation diagram of the source and antenna being used. For example, for a directional source with a narrow beam of width $\Delta\theta$, Ω_A is given as

$$\Omega_A = \int_{\phi=0}^{2\pi} \int_{\theta=0}^{\Delta\theta} \sin\theta d\theta d\phi = 2\pi \ (1 - \cos\Delta\theta). \quad (6)$$

In light of the existing THz and optical sources (see Sec. III), a more realistic approach would be to consider a light source with a Gaussian beam which has a radiation pattern given by [17]

$$E_\theta = \frac{1}{2}(1 + \cos\theta). \quad (7)$$

Since the radiated power, P, is proportional to $|E_\theta|^2$ according to $P = |E_\theta|^2/2\eta$ [16], where η is the wave impedance in the specific human tissue medium, the solid angle, Ω_A, of a Gaussian beam of width $\Delta\theta$ is given as

$$\Omega_A = \int_{\phi=0}^{2\pi} \int_{\theta=0}^{\Delta\theta} \frac{1}{4}(1 + 2\cos\theta + \cos^2\theta)\sin\theta d\theta d\phi$$
$$= \frac{\pi}{2}\left[\frac{8}{3} - (\cos\Delta\theta + \cos^2\Delta\theta + \frac{1}{3}\cos^3\Delta\theta)\right]. \quad (8)$$

B. Intrabody Path Loss Due to Molecular Absorption by Human Tissue

Molecules present in a standard medium are excited by electromagnetic waves at specific frequencies within the THz band and optical window. Molecular vibration of excited molecules occurs when atoms in a molecule are in periodic motion while the molecule as a whole has constant translational and rotational motion [18]. It must be noted that both the THz and

optical waves are non-ionizing in which they induce vibration, but cannot break molecules. Due to this vibration, part of the energy of the propagating wave is converted into kinetic energy or, from the communication perspective, simply lost. Hence, molecular absorption is calculated by computing the fraction of the incident electromagnetic radiation that is able to pass through the medium at a given frequency. Using the Beer-Lambert law [19], attenuation due to molecular absorption for an EM traveling wave at a distance, d, is given by

$$L_{abs} = e^{-\mu_{abs} d}, \tag{9}$$

where μ_{abs} is the molecular absorption coefficient. This coefficient depends on the composition of the medium and was first introduced and computed for gas molecules by Jornet et al. in [20]. In the context of intrabody communications, the same approach is followed since the body is composed of nanoscale biomolecular structures. These include chromophores, which are compounds in our tissues responsible for absorbing light radiation. Each molecule has a spectrum of absorption that can quickly change even for small wavelength variations. The disruption of the medium optical uniformity can be expressed in the non-uniformity of the refractive index throughout the medium [21]. Hence, the molecular absorption coefficient can be calculated using

$$\mu_{abs} = \frac{4\pi (n'')}{\lambda_g}. \tag{10}$$

To estimate the absorption coefficient, we can follow two different strategies. On the one hand, we can model the absorption from individual particles. The efficiency of a particle to absorb radiation can be expressed by the absorption efficiency

$$Q_{abs} = \sigma_{abs}/\sigma_g, \tag{11}$$

where σ_{abs} is the molecular absorption cross section, and $\sigma_g = \pi r^2$ is the geometric cross section. The absorption coefficient μ_{abs} can be then obtained as

$$\mu_{abs} = \rho_v Q_{abs} \sigma_g, \tag{12}$$

where $\rho_v = \kappa/(\frac{4}{3}\pi r^3)$ is the particle concentration, and κ is the volume fraction of the particle. At this stage, the main challenge is to estimate the value of Q_{abs}. This is a rather complex task, specially when different types of molecules with different frequency responses are considered.

On the other hand, provided that we are dealing with a large number of molecules, it is common to consider the effective medium assumption. In particular, the dielectric response in the frequency domain of tissues having high water content can be characterized by the Debye Relaxation Model [22], which describes the reorientation of molecules that could involve translational and rotational diffusion, hydrogen bond arrangement, and structural rearrangement. For a pure material, multiple Debye processes are possible where the complex permittivity is described by [23]

$$\epsilon = \epsilon_\infty + \sum_{j=1}^{n} \frac{\Delta\epsilon}{1 + jw\tau_j}, \tag{13}$$

where ϵ_∞ is the permittivity at the high frequency limit, $\Delta\epsilon = \epsilon_j - \epsilon_{j+1}$, ϵ_j are intermediate values, occurring at different

TABLE I
PERMITTIVITY AND RELAXATION TIME VALUES

Model	ϵ_∞	ϵ_1	ϵ_2	τ_1(ps)	τ_2(ps)
Water [22]	3.3	78.8	4.5	8.4	0.1
Whole Blood [25]	2.1	130	3.8	14.4	0.1
Skin [22]	3.0	60.0	3.6	10.6	0.2

permittivity relaxations, τ_j is the relaxation time relating to the jth Debye type relaxation process, and w is the angular frequency given as $2\pi f$.

The disordered nature and microstructure of biological matter as well as the supracellular organization in such materials, often taking the form of fractal structures, trigger different polarization mechanisms which include multiple relaxation times and non-symmetric time-domain response.

To provide the best approximation of complex permittivity for polar liquids at frequencies up to 1 THz, the double Debye equations are used [24]

$$\epsilon = \epsilon_\infty + \frac{\epsilon_1 - \epsilon_2}{1 + jw\tau_1} + \frac{\epsilon_2 - \epsilon_\infty}{1 + jw\tau_2}. \tag{14}$$

Equation (14) is rationalized and the real and imaginary parts of the complex permittivity are separated as follows

$$\epsilon' = \epsilon_\infty + \frac{\epsilon_1 - \epsilon_2}{1 + (w\tau_1)^2} + \frac{\epsilon_2 - \epsilon_\infty}{1 + (w\tau_2)^2}, \tag{15}$$

$$\epsilon'' = \frac{(\epsilon_1 - \epsilon_2)(w\tau_1)}{1 + (w\tau_1)^2} + \frac{(\epsilon_2 - \epsilon_\infty)(w\tau_2)}{1 + (w\tau_2)^2}. \tag{16}$$

Using the values in Table I, ϵ' and ϵ'' are computed. These values are then used to calculate (10) in order to find the attenuation due to molecular absorption, L_{abs}, given in (9) at the THz band. It is to be noted that the characterization of the Debye parameters for human fat at the lower THz frequencies is not available in the literature according to authors' knowledge [22], [25].

Moving towards the near-infrared frequency, particularly the optical window, catalogues of human tissue optical properties available in the literature are used [12], [26]. The detailed wavelength and corresponding permittivity are provided in Table II. Similar to the approach illustrated above, these values will be used to calculate (10) in order to find attenuation due to molecular absorption, L_{abs}, given in (9) at the optical window.

It must be noted that the human skin is composed of the epidermis, dermis as well as hypodermis. The epidermis forms the outermost layer, providing an initial barrier to the external environment. It is composed 95% of keratinocytes but also contains melanocytes [27]. Beneath this, the dermis comprises two sections, the papillary and reticular layers, and contains connective tissues, vessels, glands, follicles, hair roots, as well as sensory nerve endings. The hypodermis is the innermost and thickest layer of the skin. It invaginates into the dermis and is attached to it by collagen and elastin fibers. The hypodermis is essentially composed of a type of cells specialized in accumulating and storing fats, known as adipocytes [28]. Hence, the permittivity values of fat could be

$\lambda(nm)$	Fat	Hemoglobin	Water
450	2.13-j6.68×10^{-7}	2.04-j3.46×10^{-3}	1.78-j2.72×10^{-9}
500	2.13-j2.20×10^{-7}	2.03-j1.26×10^{-3}	1.78-j2.68×10^{-9}
550	2.13-j9.89×10^{-8}	2.01-j2.86×10^{-3}	1.77-j5.35×10^{-9}
600	2.13-j6.47×10^{-8}	1.99-j2.50×10^{-4}	1.77-j2.91×10^{-8}
650	2.13-j7.12×10^{-8}	1.99-j2.87×10^{-5}	1.77-j4.36×10^{-8}
700	2.13-j5.26×10^{-8}	1.99-j2.43×10^{-5}	1.77-j9.22×10^{-8}
750	2.13-j1.70×10^{-7}	1.99-j4.68×10^{-5}	1.76-j4.14×10^{-7}
800	2.13-j7.45×10^{-8}	1.99-j7.83×10^{-5}	1.76-j3.35×10^{-7}
850	2.13-j1.26×10^{-7}	1.99-j1.08×10^{-4}	1.76-j7.81×10^{-7}
900	2.13-j9.66×10^{-7}	1.99-j1.29×10^{-4}	1.76-j1.33×10^{-6}
950	2.13-j8.69×10^{-7}	1.99-j1.37×10^{-4}	1.76-j7.79×10^{-6}
1000	2.13-j6.17×10^{-7}	1.99-j1.23×10^{-4}	1.76-j7.67×10^{-6}

used for skin since the hypodermis is the layer that plays the most important role in skin absorption [29].

C. Intrabody Path Loss Due to Scattering by Human Tissue

From the nanosensor perspective, the body is a collection of different types of composites, such as cells, organelles, proteins, and molecules with different geometry and arrangement as well as different electromagnetic properties. Scattering by particles affect the propagation of the electromagnetic wave due to the deflection of the beam caused by the microscopic non-uniformities present in the human body. This propagation phenomenon depends on the size, shape, and refractive index of the individual particle as well as on the wavelength of the incident beam [30]. Rayleigh and Mie theories describe the scattering processes on small spherical objects. When the scattering particle diameters are smaller than the wavelength of the propagating electromagnetic wave, Rayleigh scattering occurs. On the other hand, when the particle diameters are approximately equal to the wavelength of the electromagnetic wave, Mie scattering takes place [31]. When the objects are large compared to wavelength, specular, or geometric scattering occurs [32]. The effect of scattering is analyzed using the geometry of Fig. 1, which shows a plane wave incident on a scatterer object placed at the origin of a spherical coordinate system (r, θ, ϕ).

The most important characteristic of a scattered wave is its intensity, I_{sca}, expressed as [33]

$$I_{sca} = \frac{1}{(kr)^2} I_{inc} S(\theta, \phi), \tag{17}$$

where $k = 2\pi/\lambda$ is the wave number of the incident radiation, I_{inc} is the incident intensity, and $S(\theta, \phi)$ is the scattering amplitude function. In general, $S(\theta, \phi)$ depends on the wavelength of the incident beam and on the size, shape, and optical properties of the particle [33].

In addition to the intensity function, the scattering cross section and the scattering efficiency are needed to characterize the scattering loss. The scattering cross section, σ_{sca}, is defined as the ratio between the power scattered by the particle and
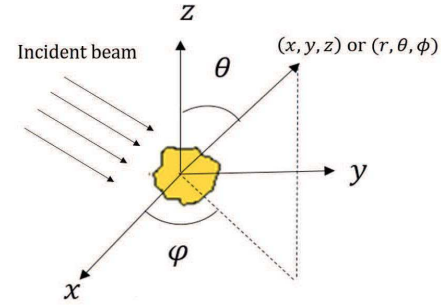

Fig. 1. Geometry of a scattering scenario showing the coordinates of both Cartesian and spherical coordinate systems.

the incident power per unit area, and is given by

$$\sigma_{sca} = \frac{1}{(k)^2} \int_0^{2\pi} \int_0^{\pi} |S(\theta, \phi)|^2 \sin\theta d\theta d\phi, \tag{18}$$

where the scattering amplitude function, $S(\theta, \phi)$, of a sphere, that mimics a particle, is given by

$$S(\theta, \phi) = \frac{k^2}{4\pi} \int_{\mathfrak{A}} e^{-ik\xi\sin\theta(\xi\cos\phi+\eta\sin\phi)} (1 + \cos\theta) d\xi d\eta, \tag{19}$$

in which $\mathfrak{A}$ is the planar aperture. Since both a sphere and an opaque disk have the same diffraction pattern, the scattering amplitude of a disk is considered for simplicity as it is independent of the azimuthal angle ϕ

$$S(\theta) = \frac{k^2}{4\pi} \int_{\mathfrak{A}} e^{-ik\xi\sin\theta} (1 + \cos\theta) d\xi d\eta. \tag{20}$$

The integral evaluation is present in [34].

Analogous to absorption, the scattering efficiency, Q_{sca}, represents the ratio of the energy scattered by the particle to the total energy in the incident beam intercepted by the geometric cross section of the particle and is given by

$$Q_{sca} = \sigma_{sca}/\sigma_g. \tag{21}$$

These values depend largely on the size of the particles. In our model, we consider the scattering from both small molecules as well as relatively large cells.

1) Scattering by Particles: For particles much smaller than the wavelength, the local electric field produced by the wave is approximately uniform at any instant. This applied electric field induces a dipole in the particle. Because the electric field oscillates, the induced dipole oscillates; and according to classical theory, the dipole radiates in all directions. This type of scattering is called *Rayleigh scattering* [35].

The scattering efficiency of small spherical absorbing particles is given by [36]

$$Q_{sca}^{small} = \frac{8}{3} \psi^4 \mathbf{Re}\left(\frac{n^2 - 1}{n^2 + 2}\right)^2, \tag{22}$$

where $\psi = 2\pi r/\lambda_g$ is the dimensionless size parameter of the particle. Following a similar approach as before, we can now obtain the scattering coefficient for small particles as

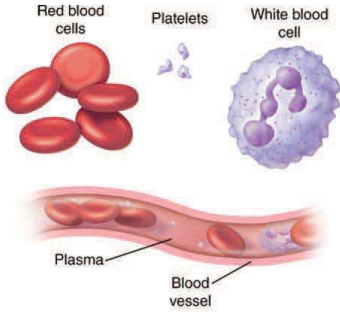$$\mu_{sca}^{small} = \rho_v Q_{sca}^{small} \sigma_g. \tag{23}$$

Fig. 2. Blood components.

2) Scattering by Cells: Scattering by large particles can be studied by applying van de Hulst approximation, which is also referred to as the anomalous diffraction approximation [36]. Indeed, the total energy removed from the incident beam, the extinction energy, is the sum of the energy scattered and absorbed. The corresponding extinction efficiency is given by [37]

$$Q_{ext} = 2 - \frac{4}{p}\sin p + \frac{4}{p^2}(1 - \cos p), \quad (24)$$

in which

$$Q_{sca}^{large} = Q_{ext} - Q_{abs}, \quad (25)$$

where $p = 4\pi r\,(n-1)/\lambda = 2(n-1)\psi$ represents the phase delay of the wave passing through the center of the particle. The complete derivation of (24) can be found in [37]. A good example where scattering from various components can be illustrated is within the human blood. As conceptually illustrated in Fig. 2, the blood is composed of various components. Blood plasma is the liquid component of the blood and is a mixture of mostly water (up to 95% by volume) and tiny particles of dissolved protein, glucose, minerals, and so forth. It also holds different types of blood cells in suspension, which are considered as the larger particles of the blood, namely, platelets (2 microns in diameter), red blood cells (7 microns), and white blood cell (up to 20 microns).

Combining (25) and (24) in (23), we can now obtain the scattering by large particles as

$$\mu_{sca}^{large} = \rho_v Q_{sca}^{large} \sigma_g. \quad (26)$$

Based on light theory, a large particle removes from the beam twice the amount of the light intercepted by its geometric cross section. For a light interacting with a large particle, the incident beam can be considered to consist of a set of separate rays. Of those rays passing within an area defined by the geometric cross section of the sphere, some will be reflected at the particle surface and others refracted. All of the energy incident on the particle surface is removed from the beam by scattering or absorption, accounting for an efficiency factor of unity. There is, however, another source of scattering from the incident beam. The intensity distribution within the diffraction pattern depends on the shape of the perimeter and size of the particle relative to the wavelength of the light. The total amount of energy that appears in the diffraction pattern is equal to the energy in the beam intercepted by the geometric

cross section of the particle. Hence, the total efficiency factor based on the cross-sectional area is equal to 2 [38]. This effect will be demonstrated and further examined in the numerical results section.

Finally, attenuation due to scattering is obtained from the addition of the scattering coefficient for both large and small particles, and is given as

$$L_{sca} = e^{-(\mu_{sca}^{small} + \mu_{sca}^{large})d}, \quad (27)$$

where d is the propagation distance.

The Beer-Lambert (BL) law can be interpreted in the literature in two different ways. One approach assumes that BL accounts for the combined effect of absorption and scattering [39]. However, in our analysis, we adopted a form of BL law that separates the effect of absorption from scattering in line with [40]. The latter approach is more appropriate in our scenario since for the absorption case, the effective medium assumption is made due to the large number of molecules available in the medium. However, in the case of scattering, we have small as well as large cells, and the effective medium assumption that entails the use of BL law is not valid anymore.

III. TERAHERTZ AND PHOTONICS FOR COMMUNICATION TECHNOLOGIES

In any communication system design, link budget analysis is the essential starting point for estimating the different losses encountered as the signal propagates from the transmitter to the receiver. A comprehensive and accurate model that predicts all the losses within the communication link is important for predicting the required transmitter power as well as the required receiver sensitivity. In RF system design, link budget estimations have been studied extensively, ranging from several hundred MHz for RFIDs [41], [42] up to several THz for broadband wireless [43]. However, in the context of intrabody communication, the literature lacks link budget analysis between nanodevices operating within the human body. In order to perform link budget analysis, the gains and losses from the transmitter, through the medium (in this case the human body) to the receiver in a telecommunication system must be taken into account.

It is important to emphasize that this paper affirms the feasibility of electromagnetic communication amongst nanodevices by providing both accurate characterization of the intrabody channel as well as presenting recent advancements in the THz/optical transmitter and receiver technologies. Since intrabody communication is concerned with nanoscale sensors, our link budget analysis is carried out for the propagation phenomena at the THz band as well as optical window.

The link budget equation is given as

$$P_R(\textbf{dB}) = P_T + G_T - Losses + G_R, \quad (28)$$

where P_R and P_T are the received and transmitted powers, respectively. G_T and G_R are the gains of the transmitting and receiving antennas, respectively. The following subsections discuss signal generation at both THz and optical frequencies, followed by addressing signal reception and detection mythodologies at the aforementioned frequencies. Using the analysis

TABLE III
CHARACTERISTICS OF TERAHERTZ TRANSMITTERS

Terahertz Transmitters	Operation Frequency	Regime	Output Power	Reference
Monolithic Integrated Circuits	$0.1 - 0.67$ THz	Pulse	few mW	[51]
Difference Frequency Generation	$0.1 - 3$ THz	CW or Pulse	few mW - 100 mW	[52]
High Electron Mobility Transistors	0.15 THz	CW or Pulse	20 mW	[53] [54]
Terahertz Photo-mixer	0.3-3 THz	CW	several tens of μW	[55]
Antenna-coupled SiGe HBT	0.49 THz	CW	38 μW	[56]
Photoconductive Antenna	0.1-2.5 THz	Pulse	1.4 mW - 90 mW	[57]

TABLE IV
CHARACTERISTICS OF OPTICAL TRANSMITTERS

Optical Transmitters	Pumping Method	Power Conversion Efficiency	Output Power	Reference
Semiconductor Lasers	Direct Pumping	up to 80%	few mW - 0.5 W	[58]
Fabry-Perot Diode Lasers	Electrical Pumping	$\sim 50\%$	1 mW - 200 mW	[59]
Light Emitting Diodes (LEDs)	—	up to 70%	10mW - 2000 mW	[60] [27]
Plasmonic Laser Antennas	Laser Pumping	—	30 mW	[61]
Optical Antennas	Laser Pumping	up to 7%	1 mW	[62] [63]

results, the power, dynamic range, noise level specification, as well as the signal waveform parameters can be determined.

A. Terahertz Transmitters

For many years, the lack of efficient methods to generate THz band signals has limited the feasibility of THz band communication networks. However, the refinement of existing architectures and the utilization of new technologies brought this paradigm one step closer in which an outstanding progress has been witnessed towards the development of these devices [44]. In order to enable communication among nanoscale devices, THz transmitters are ought to be compact where their area size should reach several hundreds of square nanometers or few square micrometers at most. They should be fast in order to support modulation bandwidths of at least several gigahertz (GHz). In addition, these sources must be energy efficient and preferably tunable [45].

Table III demonstrates the various THz transmitters available in the literature. It could be deduced that electronic sources exhibit several design and performance features that make them feasible for THz biological research studies. Indeed, they are capable of providing high levels of average output power at lower THz frequencies [46]. Moreover, they generate narrow linewidth continuous THz radiation. They are also rugged, compact, and operate at room temperature [47].

In addition to ultra-high-speed transmitters, ultra-broadband antennas are needed to enable multi-gigabit per second (Gbps) and Terabit per second (Tbps) links in the THz band. In fact, the potential of novel antennas based on nanomaterials and metamaterials needs to be investigated. For example, it has been shown that graphene can be used to build plasmonic nano-antennas, which exploit the behavior of global oscillations of surface charges to radiate in the THz band. The response of graphene-based nano-antennas can be easily dynamically tuned by means of material doping, that is,

dynamically changing the electrical properties by means of electrostatic bias [5]. Their very small size also enables their integration in virtually everything. The expectedly very low gain and effective area of individual THz band antennas motivates the investigation of very large antenna arrays. An open challenge is to characterize and account for the interaction and coupling effects among nearby antennas [44].

Advancements in microelectronics led to miniature electronic components suitable for intrabody communication. For instance, novel miniaturized transistors that adopt non-planar architectures, such as the FinFET [48] and the 3D Tri-gate transistor [49], have been manufactured. Beside their compact size, these architectures mitigate the undesirable behavior of the short channel effect and increase the transistor channel dimension. Such features resulted in reducing the transistor size to 14 nm [48], leading to higher transistor density chips, which are essential for the deployment of nanobiosensors for intrabody communication.

B. Optical Transmitters

Frequencies covering the optical frequency window, roughly between 400 THz and 750 THz, require photonic sources in order to be generated. In optical communications, light sources must be compact, monochromatic, stable, and long lasting. The two most commonly used optical sources are laser diodes and light-emitting diodes (LEDs) [70]. Actually, over the past years, these technologies witnessed progress where scientists have investigated and developed many types of lasers and LEDs enabling simple, inexpensive, and high performance optical transmission. The former transmitter falls into several broad categories, namely solid, liquid (DYE), and gas lasers, while the latter involve ultraviolet, infrared, and broadband LEDs. However, only compact, room-temperature transmitters can be utilized in biological applications; therefore, most

TABLE V
CHARACTERISTICS OF TERAHERTZ DETECTORS

Terahertz Detectors	Responsivity	Noise Equivalent Power (W/$\sqrt{\text{Hz}}$)	Reference
Bolometers	40 V/W	$< 1 \times 10^{-12}$	[64]
Schottky Diodes	400 V/W	$\approx 1.5 \times 10^{-12}$	[65]
Si-based CMOS	2.85 A/W	$1 \times 10^{-10} - 1 \times 10^{-12}$	[66]
HEMT	5 A/W	$1 \times 10^{-10} - 1 \times 10^{-12}$	[66]
Antenna-coupled graphene FETs	0.1 V/W	1×10^{-15}	[67]
Graphene-based photo-thermoelectric detector	715 V/W	16×10^{-12}	[68]

TABLE VI
CHARACTERISTICS OF OPTICAL DETECTORS

Optical Detectors	Responsivity	Noise Equivalent Power (W/$\sqrt{\text{Hz}}$)	Reference
Pyroelectric Detectors	$3 \cdot 7 \times 10^5$ V/W	1×10^{-9}	[69]
Silicon Photodiodes	0.9 A/W	$1 \times 10^{-12} - 1 \times 10^{-15}$	[70]

optical sources employed in practical systems are semiconductor based [71]. Table IV illustrates the characteristics of the different optical transmitters. Similar to THz transmitters, the compact size is a critical design requirement for optical transmitters. Nanoscale semiconductor plasmon lasers as small as $200 \times 200 \times 420$ nm^3 have been presented in [72].

C. Terahertz Receivers

The detection of THz radiation is resistant to the commonly employed techniques in the neighboring microwave and infrared (IR) frequency bands. These detectors should be able to exploit the very large available bandwidth at THz band frequencies, while providing high detection sensitivity, and low noise figures needed to overcome the very high path loss at THz frequencies. Actually, progress in THz detector sensitivity has been impressive in a period of more than half century in which the noise equivalent power (NEP) value has decreased by a factor of 10^{11} in 70 years, corresponding to an improvement by a factor of two every two years [73]. Depending on the type of detector, the maximum received measurable power can be in the mW or μW range [74]. Table V demonstrates the properties of the various Terahertz detectors available in the literature.

Similar to transmitters, miniature receivers are required to initiate an intrabody communication link. Small scale THz detectors not only include nanometric transistors [48] and diodes [75] but also bolometers occupying an area as small as 75×75 μm^2 presented in [76].

D. Optical Receivers

Applications in the photonics field require the use of optical radiation detectors. The two main types of optical detectors are thermal detectors and photon detectors as illustrated in Table VI. Thermal detectors convert the optical energy to heat energy, which then generates an electrical signal. On the other hand, photon detectors produce one electron for each incoming photon of optical energy where the electron

is detected by an electronic circuitry [77]. Several types of photon detectors exist including PIN photodiode, avalanche photodiode (APD), Schottky photodiode as well as quantum well and quantum dot detectors. In practice, silicon photodiodes have become the detector of choice for many photonic applications within their spectral range [69]. Developments in optical technologies resulted in considerate detectors feasible for intrabody communication. For instance, pyroelectric detectors have an effective aperture between 1.5 to 9 mm [74].

IV. NUMERICAL RESULTS

In this section, we numerically evaluate the analytical models for spreading, absorption and scattering presented in Sec. II, by taking into account realistic parameters of the intrabody properties (summarized in Tables I and II). In this first work, we conduct our analysis for the main body constituents where we consider a homogeneous medium composed of water, blood as well as skin or fat.

A. Spreading Loss

Figs. 3 and 4 demonstrate the spreading loss associated with THz and optical intrabody wave propagation, respectively. Similar to conventional communication models in the megahertz or few gigahertz frequency ranges, the spreading loss increases with both distance and frequency.

B. Molecular Absorption

Fig. 5 illustrates the variation of the molecular absorption coefficient, μ_{abs}, provided in (12), for different human tissues at THz frequencies. It is evident from Fig. 5 that the effect of molecular absorption is more dominant in blood compared to other types of human tissues, which is expected since blood plasma is the liquid component of blood contributing to 55% of the body total blood volume [78]. It must be noted that the reason behind the high absorption in the THz band is the fact that the rotation transition of water molecules is located in this band.
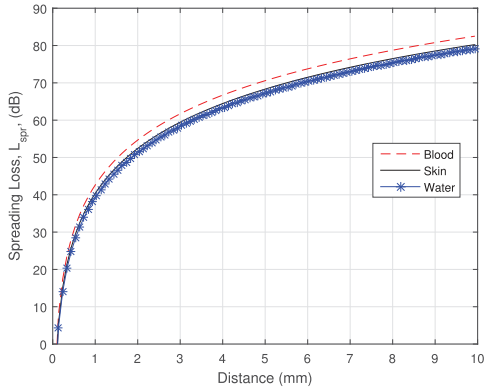
Fig. 3. Spreading loss factor, L_{spr}, at ($\lambda = 300$ μm), when short range communication between (0,01 mm-10 mm) is considered.
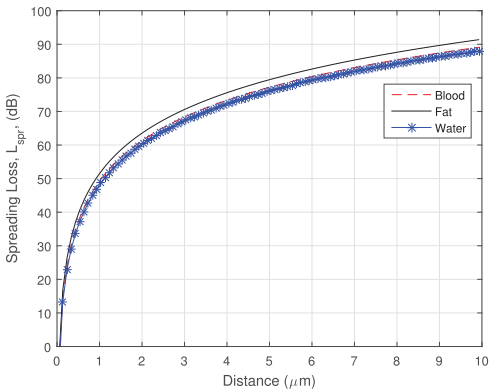

Fig. 4. Spreading loss factor, L_{spr}, at ($\lambda = 600$ nm), when short range communication between (0,01 μm-10 μm) is considered.
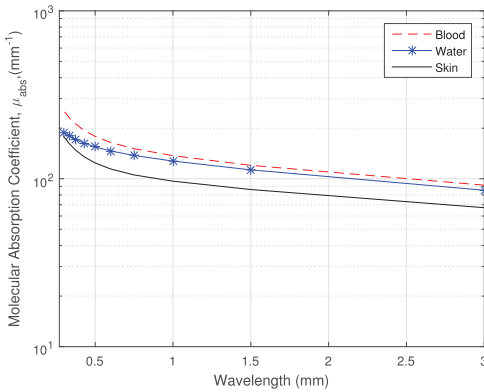

Fig. 5. Molecular absorption coefficient, μ_{abs}, for different human tissues vs. wavelength at THz ($\lambda = 300$ μm to 3 mm).

Unlike the high absorption in blood at THz frequencies, Fig. 6 demonstrates that molecular absorption in blood reduces by one order of magnitude at optical frequencies, roughly between 400 and 750 THz, compared to its value at the lower THz band. It can also be noticed that as the frequency increases to the optical band, the wavelength of the propagating wave becomes comparable to the cell size. Therefore, molecular absorption in blood cells is four orders of magnitude higher than its value of water as noticed from Fig. 6. Hence, chromophores, namely hemoglobin, play the main absorbing role in blood.
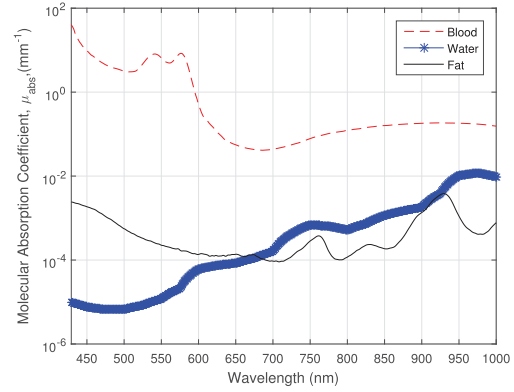

Fig. 6. Molecular absorption coefficient, μ_{abs}, for different human tissues vs. wavelength at optical window ($\lambda = 450$ nm to 1000 nm).

Body Components	Radius (m)
Water Particle	1.4×10^{-10}
Red Blood Cell	4×10^{-6}
Skin Cell	30×10^{-6}
Adipocyte (Fat Cell)	50×10^{-6}

One of the challenges that arises due to the absorption effect is the fact that it triggers the vibration of cells which in turn results in heat generation. The thermal effect will be thoroughly investigated in further publications where a mathematical framework will be presented to illustrate how molecules in the human body absorb energy from electromagnetic fields and subsequently release this energy as heat to their immediate surroundings. As a result, a change in temperature is witnessed from which the molecular absorption noise is calculated.

C. Scattering

As for the effect of scattering, (23) and (26) can be used taking into consideration the radii of the various body particles as given by Table VII. It should be noted that the size of the scatterers at THz is much smaller than the wavelength of the propagating THz wave. Results of the scattering coefficient, μ_{sca}, given in Fig. 7 is almost negligible compared to its counterpart, absorption, given in Fig. 5. This finding makes sense because the scattering effect is only significant for wavelengths that are much smaller than scatterer dimensions, unlike the current case in which we are investigating scattering at the THz wavelengths. This adds to the advantages of incorporating the THz band for intrabody communication because the propagating signal will not suffer from the scattering effects which are more significant in the higher optical frequencies. Based on the above finding, only the spreading and absorption losses contribute to the total path loss at THz frequencies.

The in-vivo scattering effects have also been analyzed for optical frequencies with results presented in Fig. 8. Comparing the results of Fig. 7 and Fig. 8, one can conclude that the scattering effect is dominant in the latter figure which is
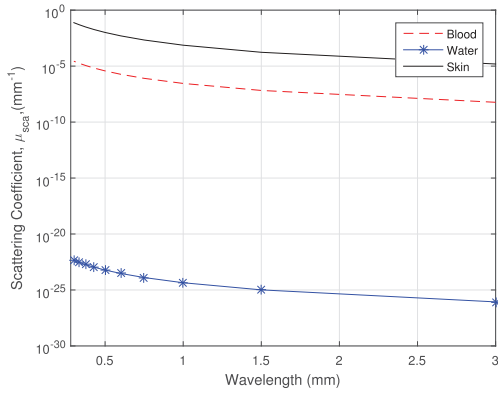
Fig. 7. Scattering coefficient, μ_{sca}, for different human tissues vs. wavelength at THz ($\lambda = 300\ \mu m$ to $3\ mm$).
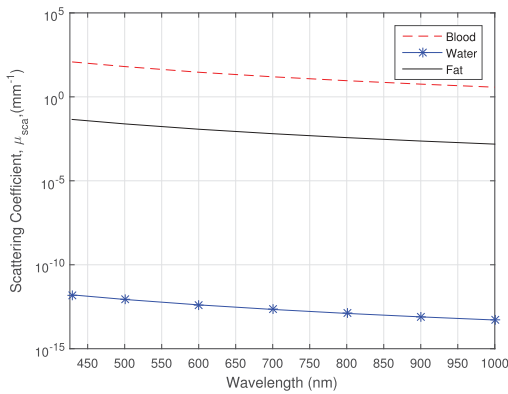

Fig. 8. Scattering coefficient, μ_{sca}, for different human tissues vs. wavelength at optical window ($\lambda = 450\ nm$ to $1000\ nm$).

Fig. 9. Scattering efficiency of a blood particle at $\lambda = 450\ nm$.

Fig. 10. Electric field intensity (V/m) of a circular cross section composed of a three-layer human tissue: COMSOL Multiphysics simulation model.

obtained for optical frequencies. This confirms the conclusion obtained in the preceding paragraph. The effect of scattering at optical frequencies has been further investigated by calculating the scattering efficiency as a function of the particle radius. Results are presented in Fig. 9 which shows that the scattering amplitude at optical frequencies resembles a decaying sinusoid. The results of Fig. 9 will help us predict the scattering effect due to various blood cell types, having different sizes. It can be inferred that as the particle size parameter ψ becomes much larger than 1, the scattering efficiency approaches 2, which come to an agreement with classical optical principles. Thus, when blood cells are considered, there is scattering created by their large size, then absorption within the cell.

An important observation to be made is whether we are operating in the near-field or far-field region of the antenna. Actually, based on the Fraunhofer distance [16], if the value of ($\frac{2\pi}{\lambda} r \gg 1$), we will be operating in the far-field of the antenna; otherwise, the near-field interaction of waves will be in effect. At the optical frequencies, with a wavelength of 600 nm, a transmission distance of 1 μm ensures operation in the far-field region. However, when dealing with THz frequencies, the transmission distance must be greater than 100 μm for the far-field assumption to be valid. Nevertheless, as a first estimation, the Rayleigh-Gans-Debye scattering theory provides an adequate approximation for the scattering effect, regardless of the transmission distance [80].
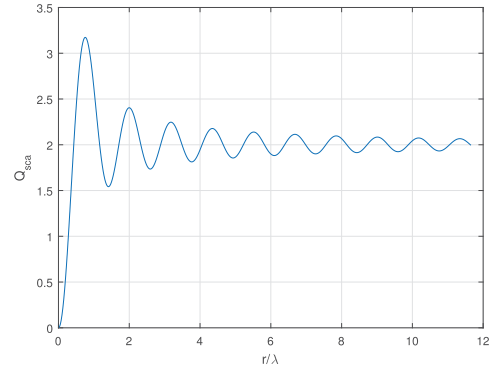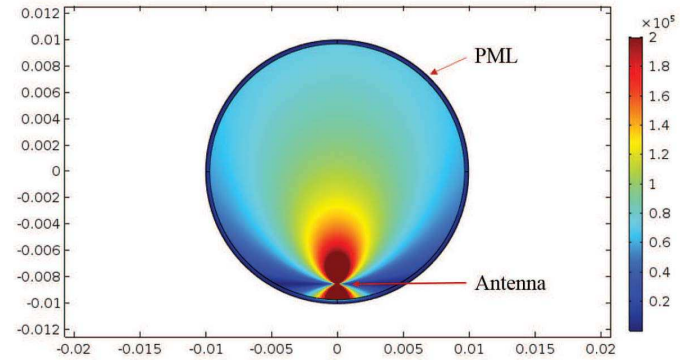
D. Path Loss

In this subsection, the theoretical model is validated using COMSOL Multiphysics. A homogeneous medium with the same parameters that are used for the theoretical model has been taken to account by considering a circular cross section composed of the three main layers of human tissues, namely, skin, blood and water. A point dipole antenna is chosen as the electromagnetic wave radiation source and the wave propagation has been simulated for up to 10 mm and 10 μm far from the antenna for the THz and optical frequencies, respectively. The radiated power by a dipole antenna can be written as

$$P_{rad} = (\pi\eta/3)|I_0 l/\lambda|^2, \tag{29}$$

where I_0 is the input current, l is the antenna length and the product $I_0 l = 1$. The whole medium is enclosed by a perfect matched layer (PML). The PML is utilized to mimic the infinite environment and its thickness is half wavelength. The graphical representation of the model is demonstrated in Fig 10.

The total path loss between two nanodevices operating at the THz frequency given in (1) is presented in Fig. 11 for a short range communication scenario. It can be seen that the developed model agrees with the FEM simulation which proofs that the model is accurate enough. It must be highlighted that due to recent advancements in THz technologies, novel THz transmitters and receivers have been developed facilitating the communication between nanodevices and
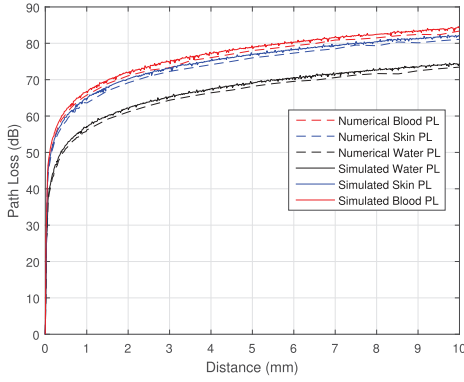
Fig. 11. Total path loss factor, L_{tot}, at ($\lambda = 300$ μm), when short range communication between (0,01 mm to 10 mm) is considered.

Fig. 12. Total path loss factor, L_{tot}, at ($\lambda = 600$ nm), when short range communication between (0,01 μm-10 μm) is considered.

opening the door to potentially biocompatible applications of iWNSNs. On the other hand, Fig. 12 indicates the path loss experienced at the optical frequency window, in which we can see that both the numerical and simulated results agree. The presented scenarios are fundamental for the analysis of intrabody communication. Depending on the application, the user may choose at which frequency and distance the EM signal should be transmitted.

E. Link Budget Analysis

As mentioned in Sec. III, wireless systems are required to provide a certain minimum transmission quality. Hence, link budget is the clearest and most intuitive way of computing the required transmit power. It actually tabulates all equations that connects the transmitted power to the received Signal to Noise Ratio (SNR) [81].

1) THz Band: The path loss at 1 THz for propagating a distance of 1 mm into blood is 65.8 dB, as obtained from Fig. 11. From Table III, a value of 1 mW (-30 dBW) has been chosen as transmit power.

The received power given in (28) is

$$P_R(\textbf{dB}) = -30 - 65.8 = -95.8. \qquad (30)$$

This value is equivalent to 263 pW. Assuming an SNR value of 10 dB,

$$SNR = P_R - N$$
$$10 = -95.8 - N \qquad (31)$$

Hence, a minimum receiver sensitivity value of -105.8 dBW (26.3 pW) is required. Based on Table V, various receivers capable of detecting the incoming signal exist. This verifies the feasibility of intrabody communication in the THz band.

2) Optical Window: The path loss at 499 THz (600 nm) for propagating a distance of 10 μm into blood is 88.6 dB, as deduced from Fig. 12. This propagation distance is chosen to ensure that a viable optical link is established. From Table IV, a value of 100 mW (-10 dBW) has been chosen as transmit power, considering a compromise between the achievable transmit powers of the various technologies
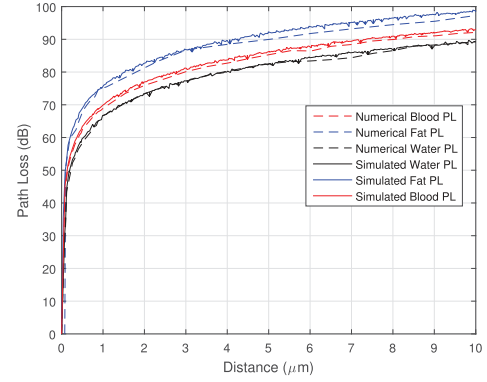
TABLE VIII
GAIN EFFECT ON LINK BUDGET CALCULATION

Range of Operation	P_R (W)	Receiver Sensitivity
THz Band	708 pW	70.8 pW
Optical Window	371.5 pW	37.1 pW

available. Therefore, the received power given in (28) is

$$P_R(\textbf{dB}) = -10 - 88.6 = -98.6, \qquad (32)$$

which is equivalent to 138 pW. Assuming an SNR value of 10 dB,

$$SNR = P_R - N$$
$$10 = -98.6 - N \qquad (33)$$

Hence, a minimum receiver sensitivity value of -108.6 dB (13.8 pW) is required. Based on Table VI, silicon photodiodes will be capable of detecting the incoming signal, which proves the feasibility of the intrabody communication scenario.

It must be noted that the optical sources described in Table IV are highly directional which translates into gains up to 15 dB depending on the beam width, $\Delta\theta$, of (8), provided in Sec. II. This results in extending the intrabody propagating distance to few millimeters. However, in order to make a fair comparison with the THz Band, the results obtained assume omnidirectionality for both technologies.

3) Effect of Gain: An antenna's gain is a key performance which combines the antenna's directivity and electrical efficiency. As a transmitting antenna, the gain describes how well the antenna converts input power into radio waves headed in a specified direction. As a receiving antenna, the gain describes how well the antenna converts radio waves arriving from a specified direction into electrical power [16]. The previously presented link budget calculations have been repeated by taking into account the antenna gain value of 2.15 dBi, as it corresponds to a half-wavelength dipole antenna. Hence, a total gain of 4.3 dBi has been added based on (28) corresponding to the antenna transmit and receive gains, respectively. The results are presented in Table VIII. It can be stemmed that even by taking into account the antenna gain, both THz and photonic technologies are capable of capturing the propagating signal through the body.

V. CONCLUSION

This paper developed a channel model for predicting the effect of THz and optical bio-electromagnetic propagation. The presented model is novel since it takes into account the combined effect of three main propagation phenomena encountered in intrabody communication including spreading, molecular absorption, and scattering.

The spreading effect has been accurately quantified by incorporating the directivity of the nanoantenna. Investigation of molecular absorption demonstrated that blood molecules are more absorbent in comparison to other body composites. Nonetheless, absorption from blood is one order of magnitude lower in the optical window, roughly between 400 and 750 THz. Moreover, scattering has been accurately computed by taking into account the size of the scatterer nanoparticles with respect to wavelength in both the THz band and optical frequency window. It has been also inferred that as the particle size parameter ψ becomes larger than 1, the scattering efficiency approaches 2, which come to an agreement with classical optical principles.

The combined effects of the three main propagation phenomena in intrabody communication facilitate the design and deployment of iWNSNs. The paper also provided an in depth analysis of the THz and photonic devices available in the literature. Such study is essential for conducting link budget analysis between nanodevices operating within the human body. The findings provided in this paper indicate that nano-communication based devices have the potential to play a vital role in future healthcare technologies by improving the quality of the human life.

REFERENCES

[1] I. F. Akyildiz, J. M. Jornet, and M. Pierobon, "Nanonetworks: A new frontier in communications," *Commun. ACM*, vol. 54, no. 11, pp. 84–89, Nov. 2011.

[2] R. M. Shubair and H. Elayan, "*In vivo* wireless body communications: State-of-the-art and future directions," in *Proc. Loughborough Antennas Propag. Conf. (LAPC)*, Nov. 2015, pp. 1–5.

[3] I. F. Akyildiz, F. Fekri, R. Sivakumar, C. R. Forest, and B. K. Hammer, "Monaco: Fundamentals of molecular nano-communication networks," *IEEE Wireless Commun.*, vol. 19, no. 5, pp. 12–18, Oct. 2012.

[4] G. E. Santagati, T. Melodia, L. Galluccio, and S. Palazzo, "Ultrasonic networking for e-health applications," *IEEE Wireless Commun.*, vol. 20, no. 4, pp. 74–81, Aug. 2013.

[5] J. M. Jornet and I. F. Akyildiz, "Graphene-based plasmonic nano-antenna for terahertz band communication in nanonetworks," *IEEE J. Sel. Areas Commun.*, vol. 31, no. 12, pp. 685–694, Dec. 2013.

[6] H. Elayan, R. M. Shubair, and A. Kiourti, "On graphene-based THz plasmonic nano-antennas," in *Proc. 16th Medit. Microw. Symp. (MMS)*, Nov. 2016, pp. 1–3.

[7] H. Elayan, R. M. Shubair, A. Alomainy, and K. Yang, "*In-vivo* tera-hertz EM channel characterization for nano-communications in wbans," in *Proc. IEEE Int. Symp. Antennas Propag. (APSURSI)*, Jun. 2016, pp. 979–980.

[8] M. Nafari and J. M. Jornet, "Metallic plasmonic nano-antenna for wireless optical communication in intra-body nanonetworks," in *Proc. 10th EAI Int. Conf. Body Area Netw. (ICST)*, Sep. 2015, pp. 287–293.

[9] P. Biagioni, J.-S. Huang, and B. Hecht, "Nanoantennas for visible and infrared radiation," *Rep. Progr. Phys.*, vol. 75, no. 2, p. 024402, 2012.

[10] J. Xu, K. W. Plaxco, and S. J. Allen, "Absorption spectra of liquid water and aqueous buffers between 0.3 and 3.72 THz," *J. Chem. Phys.*, vol. 124, no. 3, p. 36101, 2006.

[11] H. Guo, P. Johari, J. M. Jornet, and Z. Sun, "Intra-body optical channel modeling for *in vivo* wireless nanosensor networks," *IEEE Trans. Nanobiosci.*, vol. 15, no. 1, pp. 41–52, Jan. 2016.

[12] R. M. Pope and E. S. Fry, "Absorption spectrum (380–700 nm) of pure water. II. Integrating cavity measurements," *Appl. Opt.*, vol. 36, no. 33, pp. 8710–8723, 1997.

[13] A. G. Brolo, "Plasmonics for future biosensors," *Nature Photon.*, vol. 6, no. 11, pp. 709–713, Nov. 2012.

[14] A. Vander Vorst, A. Rosen, and Y. Kotsuka, *RF/Microwave Interaction With Biological Tissues*, vol. 181. Hoboken, NJ, USA: Wiley, 2006.

[15] P. Stavroulakis, *Biological Effects of Electromagnetic Fields*. Springer, 2003.

[16] C. A. Balanis, *Antenna Theory: Analysis and Design*. Hoboken, NJ, USA: Wiley, 2016.

[17] H. Lin, C. Fumeaux, B. M. Fischer, and D. Abbott, "Modelling of sub-wavelength THz sources as Gaussian apertures," *Opt. Exp.*, vol. 18, no. 17, pp. 17672–17683, 2010.

[18] P. Gans, *Vibrating Molecules*. London, U.K.: Chapman & Hall 1971.

[19] K. Fuwa and B. L. Valle, "The physical basis of analytical atomic absorption spectrometry. The pertinence of the beer-lambert law," *Anal. Chem.*, vol. 35, no. 8, pp. 942–946, 1963.

[20] J. M. Jornet and I. F. Akyildiz, "Channel modeling and capacity analysis for electromagnetic wireless nanonetworks in the terahertz band," *IEEE Trans. Wireless Commun.*, vol. 10, no. 10, pp. 3211–3221, Oct. 2011.

[21] F. Martelli, S. Del Bianco, A. Ismaelli, and G. Zaccanti, "Light propagation through biological tissue and other diffusive media: Theory, solutions, and software," *Proc. SPIE*, vol. 193, p. 298, Dec. 2009. [Online]. Available: https://books.google.com/books?id=5pEDQgAACAAJ

[22] K. M. Yaws, D. G. Mixon, and W. P. Roach, "Electromagnetic properties of tissue in the optical region," *Proc. SPIE*, vol. 6435, p. 643507, Feb. 2007.

[23] J. Xu, K. W. Plaxco, and S. J. Allen, "Probing the collective vibra-tional dynamics of a protein in liquid water by terahertz absorption spectroscopy," *Protein Sci.*, vol. 15, no. 5, pp. 1175–1181, 2006.

[24] J. Kindt and C. A. Schmuttenmaer, "Far-infrared dielectric properties of polar liquids probed by femtosecond terahertz pulse spectroscopy," *J. Phys. Chem.*, vol. 100, no. 24, p. 10373, 1996.

[25] C. B. Reid, G. Reese, A. P. Gibson, and V. P. Wallace, "Terahertz time-domain spectroscopy of human blood," *IEEE J. Biomed. Health Informat.*, vol. 17, no. 4, pp. 774–778, Jul. 2013.

[26] R. L. van Veen, H. Sterenborg, A. Pifferi, A. Torricelli, and R. Cubeddu, "Determination of VIS- NIR absorption coefficients of mammalian fat, with time- and spatially resolved diffuse reflectance and transmission spectroscopy," in *Proc. Biomed. Topical Meet.*, 2004, paper. SF4.

[27] J. A. McGrath, R. A. J. Eady, and F. M. Pope, *Anatomy and Organization of Human Skin*. Oxford, U.K.: Blackwell, 2008, pp. 45–128. [Online]. Available: http://dx.doi.org/10.1002/9780470750520.ch3

[28] F. A. Duck, *Physical Properties of Tissues: A Comprehensive Reference Book*. San Diego, CA, USA: Academic, 2013.

[29] Q. H. Abbasi, H. El Sallabi, N. Chopra, K. Yang, K. A. Qaraqe, and A. Alomainy, "Terahertz channel characterization inside the human skin for nano-scale body-centric networks," *IEEE Trans. THz Sci. Technol.*, vol. 6, no. 3, pp. 427–434, May 2016.

[30] B. Chu, *Laser Light Scattering*. Amsterdam, The Netherlands: Elsevier, 1974.

[31] J. G. Calvert, "Glossary of atmospheric chemistry terms (recommenda-tions 1990)," *Pure Appl. Chem.*, vol. 62, no. 11, pp. 2167–2219, 1990.

[32] J. A. Fozard, "Diffraction and scattering of high frequency waves," Ph.D. dissertation, Jesus College Oxford Univ., Univ. Oxford, Oxford, U.K., 2005.

[33] S. Friedlander, *Smoke, Dust, and Haze: Fundamentals of Aerosol Dynamics* (Topics in chemical engineering). London, U.K.: Oxford Univ. Press, 2000. [Online]. Available: https://books.google.com/books?id=fNIeNvd3Ch0C

[34] C. F. Bohren and D. R. Huffman, *Absorption Scattering Light by Small Particles*. Hoboken, NJ, USA: Wiley, 2008.

[35] D. R. Bates, "Rayleigh scattering by air," *Planetary Space Sci.*, vol. 32, no. 6, pp. 785–790, Jun. 1984.

[36] H. C. Hulst and H. C. van de Hulst, *Light scattering by small particles*. North Chelmsford, MA, USA: Courier Corporation, 1957.

[37] A. A. Kokhanovsky, *Light Scattering Media Optics*. Springer, 2004.

[38] S. K. Friedlander, *Smoke, Dust and Haze: Fundamentals of Aerosol Behavior*, vol. 1. New York, NY, USA: Wiley, 1977, p. 333.

[39] I. Sokolik, "Basic radiometric quantities. The Beer–Bouguer–Lambert law. Concepts of extinction (scattering plus absorption) and emis-sion. Schwarzschild's equation," *Atmos. Radiat. Transf.*, no. Lecture 3, pp. 1–15, 2005.

[40] B. Mohlenhoff, M. Romeo, M. Diem, and B. R. Wood, "Mie-type scattering and non-beer-lambert absorption behavior of human cells in infrared microspectroscopy," *Biophys. J.*, vol. 88, no. 5, pp. 3635–3640, May 2005.

[41] J. D. Griffin, G. D. Durgin, A. Haldi, and B. Kippelen, "RF tag antenna performance on various materials using radio link budgets," *IEEE Antennas Wireless Propag. Lett.*, vol. 5, no. 1, pp. 247–250, Dec. 2006.

[42] J. D. Griffin and G. D. Durgin, "Complete link budgets for backscatter-radio and RFID systems," *IEEE Antennas Propag. Mag.*, vol. 51, no. 2, pp. 11–25, Apr. 2009.

[43] T. Schneider, A. Wiatrek, S. Preußler, M. Grigat, and R.-P. Braun, "Link budget analysis for terahertz fixed wireless links," *IEEE Trans. THz Sci. Technol.*, vol. 2, no. 2, pp. 250–256, Mar. 2012.

[44] I. F. Akyildiz, J. M. Jornet, and C. Han, "TeraNets: Ultra-broadband communication networks in the terahertz band," *IEEE Wireless Commun.*, vol. 21, no. 4, pp. 130–135, Aug. 2014.

[45] J. M. Jornet and I. F. Akyildiz, "Femtosecond-long pulse-based modulation for terahertz band communication in nanonetworks," *IEEE Trans. Commun.*, vol. 62, no. 5, pp. 1742–1754, May 2014.

[46] M. Feiginov, R. Gonzalo, I. Maestrojun, O. Cojocari, M. Hoefle, and E. Limiti, *THz Electronics*. Hoboken, NJ, USA: Wiley, 2015, pp. 254–303. [Online]. Available: http://dx.doi.org/10.1002/9781118920411.ch6

[47] G. J. Wilmink and J. E. Grundt, "Invited review article: Current state of research on biological effects of terahertz radiation," *J. Infr., Millim., Terahertz Waves*, vol. 32, no. 10, pp. 1074–1122, Oct. 2011.

[48] R. Borkar, M. Bohr, and S. Jourdan, "Advancing Moore's law—The road to 14 nm," Intel Corp, Santa Clara, CA, USA, Tech. Rep., 2014, vol. 14.

[49] U. E. Avci, I. Ban, D. L. Kencke and P. L. D. Chang, "Floating body cell (FBC) memory for 16-nm technology with low variation on thin silicon and 10-nm BOX," in *Proc. IEEE Int. SOI Conf.*, New Paltz, NY, USA, 2008, pp. 29–30.

[50] Q. J. Gu *et al.*, "CMOS THz generator with frequency selective negative resistance tank," *IEEE Trans. THz Sci. Technol.*, vol. 2, no. 2, pp. 193–202, Mar. 2012.

[51] P. Zhao, "Compact terahertz sources based on difference frequency generation," Ph.D. dissertation, Lehigh Univ., Pennsylvania, PA, USA, 2012.

[52] W. Knap, F. Teppe, N. Dyakonova, D. Coquillat, and J. Łusakowski, "Plasma wave oscillations in nanometer field effect transistors for terahertz detection and emission," *J. Phys., Condens. Matter*, vol. 20, no. 38, p. 384205, 2008.

[53] L. Samoska, A. Peralta, M. Hu, M. Micovic, and A. Schmitz, "A 20 mW, 150 GHz InP HEMT MMIC power amplifier module," *IEEE Microw. Wireless Compon. Lett.*, vol. 14, no. 2, pp. 56–58, Feb. 2004.

[54] T. Kleine-Ostmann, K. Pierz, G. Hein, P. Dawson, and M. Koch, "Audio signal transmission over THz communication channel using semiconductor modulator," *Electron. Lett.*, vol. 40, no. 2, pp. 124–126, Jan. 2004.

[55] P. Hillger, J. Grzyb, R. Lachner, and U. Pfeiffer, "An antenna-coupled 0.49 THz SiGe HBT source for active illumination in terahertz imaging applications," in *Proc. 10th Eur. Microw. Integr. Circuits Conf. (EuMIC)*, Sep. 2015, pp. 180–183.

[56] S.-H. Yang, M. R. Hashemi, C. W. Berry, and M. Jarrahi, "7.5% optical-to-terahertz conversion efficiency offered by photoconductive emitters with three-dimensional plasmonic contact electrodes," *IEEE Trans. THz Sci. Technol.*, vol. 4, no. 5, pp. 575–581, Sep. 2014.

[57] C. H. Henry, "Theory of the linewidth of semiconductor lasers," *IEEE J. Quantum Electron.*, vol. 18, no. 2, pp. 259–264, Feb. 1985.

[58] Y. J. Ding, "Solid-state-laser-pumped THz parametric generation and detection and applications," in *Proc. 19th Annu. Meet. IEEE Lasers Electro-Opt. Soc. (LEOS)*, Oct. 2006, p. 808.

[59] M. C. Moreira, A. Campos, and R. Prado, *Application of High Brightness LEDs in the Human Tissue and its Therapeutic Response*. Rijeka, Croatia: InTech, 2011.

[60] E. Cubukcu, E. A. Kort, K. B. Crozier, and F. Capasso, "Plasmonic laser antenna," *Appl. Phys. Lett.*, vol. 89, no. 9, p. 093120, 2006.

[61] A. Sharma, V. Singh, T. L. Bougher, and B. A. Cola, "A carbon nanotube optical rectenna," *Nature Nanotechnol.*, vol. 10, pp. 1027–1032, Sep. 2015.

[62] M. D. Wissert, *Optical Antennas: Linear and Nonlinear Excitation and Emission*. Germany: KIT Scientific Publishing, 2012.

[63] A. Rostami, H. Rasooli, and H. Baghban, *Terahertz Technology: Fundamentals and Applications*, vol. 77. Berlin, Geermany: Springer, 2010.

[64] N. Karpowicz, H. Zhong, J. Xu, K.-I. Lin, J.-S. Hwang, and X.-C. Zhang, "Non-destructive sub-THz CW imaging," *Proc. SPIE*, vol. 5727, pp. 132–142, Mar. 2005.

[65] W. Knap *et al.*, "Field effect transistors for terahertz detection: Physics and first imaging applications," *J. Infr., Millim., Terahertz Waves*, vol. 30, no. 12, pp. 1319–1337, 2009.

[66] V. Y. Kachorovskii, S. L. Rumyantsev, W. Knap, and M. Shur, "Performance limits for field effect transistors as terahertz detectors," *Appl. Phys. Lett.*, vol. 102, no. 22, p. 223505, 2013.

[67] X. Cai *et al.*, "Sensitive room-temperature terahertz detection via the photothermoelectric effect in graphene," *Nature Nanotechnol.*, vol. 9, pp. 814–819, Sep. 2014.

[68] M. Muztoba, N. Melikechi, M. M. Rana, and D. P. Butler, "Nanomachined pyroelectric detector with low thermal conductance—Design and concepts," in *Proc. IEEE SENSORS*, Nov. 2013, pp. 1–4.

[69] G. Held, *Introduction to Light Emitting Diode Technology and Applications*. Boca Raton, FL, USA: CRC Press, 2016.

[70] S. V. Vasan, *Basics of Photonics and Optics*. Bloomington, IN, USA: Trafford Publishing, 2004.

[71] S. Bhadra and A. Ghatak, Eds., *Guided Wave Optics and Photonic Devices*. Boca Raton, FL, USA: CRC Press, 2013.

[72] F. Rana, C. Manolatou, and S. G. Johnson, "Nanoscale semiconductor plasmon lasers," in *Proc. Conf. Lasers Electro-Opt. (CLEO)*, May 2007, pp. 1–2.

[73] A. Rogalski and F. Sizov, "Terahertz detectors and focal plane arrays," *Optoelectron. Rev.*, vol. 19, no. 3, pp. 346–404, 2011.

[74] *THZ-B THz Detectors and Other Products*. Accessed on Nov. 1, 2016. [Online]. Available: https://www.gentec-eo.com/products/thz-detectors

[75] L. Hong, H. Tanaka, and T. Ogawa, "Nanoscale diodes composed of single-walled carbon nanotube and physically adsorbed organic molecule nanoparticles," in *Proc. 12th IEEE Conf. Nanotechnol. (IEEE-NANO)*, Aug. 2012, pp. 1–5.

[76] J. Sikula and M. Levinshtein, Eds., *Advanced Experimental Methods for Noise Research in Nanoscale Electronic Devices*, vol. 151. The Netherlands: Springer, 2006.

[77] Z. Jakšić, *Micro and Nanophotonics for Semiconductor Infrared Detectors: Towards an Ultimate Uncooled Device*. Switzerland: Springer, 2014.

[78] D. O'Neil, *Blood Components*. San Marcos, TX, USA: Palomar College, 2012.

[79] H. P. Erickson, "Size and shape of protein molecules at the nanometer level determined by sedimentation, gel filtration, and electron microscopy," *Biol. Procedures Online*, vol. 11, no. 1, p. 32, 2009.

[80] W. J. Minkowycz, E. M. Sparrow, and J. P. Abraham, *Nanoparticle Heat Transfer and Fluid Flow*, vol. 4. Boca Raton, FL, USA: CRC Press, 2012.

[81] A. F. Molisch, *Wireless Communications*. Hoboken, NJ, USA: Wiley, 2007.

Hadeel Elayan (S'12) received the B.Sc. degree (Hons.) in electrical engineering from Khalifa University, UAE, in 2015. She is currently pursuing the M.Sc. degree in electrical engineering, on a full scholarship, with Khalifa University. She completed a Research Internship with the State University of New York, University at Buffalo, USA, in 2016. Her current research interests include Terahertz and intrabody communications, nanobiosensing, and antennas and bio-electromagnetics. She is a member of the International Society of Optics and Photonics. She received several awards for the research and she became the first student in UAE to receive the 2016 IEEE Pre-Doctoral Research Grant Award, received annually by the IEEE Antennas and Propagation Society. She was also received the 2017 Photonics School Research Internship granted by the Optical Society of America.

Raed M. Shubair (S'85–M'93–SM'01) received the B.Sc. degree (Hons.) in electrical engineering from Kuwait University, Kuwait, in 1989, and the Ph.D. degree (Hons.) in electrical engineering from the University of Waterloo, Canada, in 1993. He is a Full Professor of Electrical Engineering. He is a Visiting Scientist with the Research Laboratory of Electronics, MIT Department of Electrical Engineering and Computer Science, Massachusetts Institute of Technology (MIT), USA. He is also Full Professor of Electrical Engineering with Khalifa University, UAE, from 1993 to 2017. He has over 200 publications which include US patents, book chapters, papers in the IEEE transactions and international journals, and papers in the IEEE conference proceedings. His research interests include antennas and bio-electromagnetics, Terahertz intrabody communications, wireless nanosensor networks, Internet of Nano Things, and signal processing for wireless and medical applications. He is a member of the editorial boards of several international journals and serves regularly on the steering, organizing, and technical committees of the IEEE flagship conferences in Antennas, Communications, and Signal Processing. He conducted several tutorials and workshops in international conferences, and delivered numerous invited talks at international academic institutions. He received both the University Teaching Excellence Award and the University Distinguished Service Award several times since 1993. He was also a recipient of several international research and professional awards. These include the 2005 Distinguished Service Award from the ACES Society in USA and the 2007 Distinguished Service Award from the Electromagnetics Academy in USA. He supervised his students to receive several conference awards, including the 2015 and 2016 IEEE IIT Conference Best Selected Papers Awards, the 2015 IEEE ICCSPA Conference Best Student Paper Award, and the 2016 IEEE BioSMART Conference Best Paper Award. He also supervised his students to receive several international awards and prestigious distinctions, including the 2015 IEEE Student Travel Grants, the 2016 Vanier Canada Doctoral Research Grant Award, the 2016 IEEE Pre-Doctoral Research Grant Award, the 2016 NSF Young Professionals Award, and the 2017 OSA Photonics Research Grant Award. He has supervised and mentored his students to receive full scholarship postgraduate admissions and research internships at top universities in the USA (MIT, Harvard, Georgia Tech, and SUNY), Canada (Waterloo, UBC, Carleton, and Concordia), and in France (UPEM Paris University). He hosted invited talks by the Presidents and Distinguished Speakers of several IEEE Societies. He organized and chaired numerous technical special sessions in flagship conferences, including recently EuCAP2017 and IEEE APS2017. He serves currently as the Publicity Chair for several flagship conference, including EuCAP2017, EuCAP2018, IEEE APS2017 and IEEE APS2018, and IEEE WCNC2018. He has served as the Technical Program Chair of the IEEE MMS2016 Conference. He holds several appointments in the international professional engineering community. He was appointed and serves currently as the Chair of IEEE AP-S Educational Initiatives Committee, the Outreach Chair of the IEEE Antennas and Propagation Society, and an EuCAP Liaison for Middle East and North Africa. Most recently, he was selected to become a member of the Board for the European School of Antennas. He was also appointed as the Regional Director of the IEEE Signal Processing Society in the Middle East. He is Guest Editor of the IEEE Journal of Electromagnetics, RF, and Microwaves in Medicine and Biology. Based on his distinguished technical and professional contributions and accomplishments, he was nominated for the 2017 IEEE Distinguished Educator Award.

Josep Miquel Jornet (M'–) received the B.S. degree in Telecommunication Engineering and the M.Sc. degree in information and communication technologies from the Universitat Politécnica de Catalunya, Barcelona, Spain, in 2008, the Ph.D. degree in electrical and computer engineering from the Georgia Institute of Technology (Georgia Tech.), Atlanta, GA, in 2013. He is an Assistant Professor with the Department of Electrical Engineering, University at Buffalo, The State University of New York. From 2007 to 2008, he was a Visiting Researcher with the Massachusetts Institute of Technology (MIT), Cambridge, under the MIT Sea Grant Program. He was a recipient of the Oscar P. Cleaver Award for outstanding graduate students in the School of Electrical and Computer Engineering, Georgia Tech, in 2009. He also received the Broadband Wireless Networking Lab Researcher of the Year Award in 2010. In 2016 and 2017, he received the Distinguished TPC Member Award at the IEEE International Conference on Computer Communications, one of the premier conferences of the IEEE Communications Society. In 2017, he received the IEEE Communications Society Young Professional Best Innovation Award. Since 2016, he is the Editor-in-Chief of the *Nano Communication Networks (Elsevier) Journal*. He also serves in the Steering Committee of the ACM Nanoscale Computing and Communications Conference series. He is a member of the ACM. His current research interests are in Terahertz-band communication networks, nano-photonic wireless communication, intra-body wireless nanosensor networks and the Internet of Nano-Things.

Pedram Johari (S'11–M'–) received the B.S. degree in electrical engineering (electronics) from Azad University Central Tehran Branch, Tehran, Iran, and the M.S. degree in electrical engineering (communication systems) from the Iran University of Science and Technology, Tehran, Iran, in 2006 and 2012, respectively. He is currently pursuing the Ph.D. degree with the Department of Electrical Engineering, University at Buffalo, The State University of New York. He is currently a Graduate Research Assistant under the guidance of Prof. J. Miquel Jornet. His current research interests are in Terahertz-band communication networks, Electromagnetic nanonetworks, Nano-photonic wireless communication and Intra-Body Wireless Nanosensor Networks. From 2007 to 2014, he has been a Team Member and a Team Leader of Mobile Broad Band planning and optimization projects in several world-class wireless telecom service provider companies. He was a recipient of the Outstanding Graduate Student Award, for outstanding academic achievements in the Department of Electrical Engineering, University at Buffalo, in 2015 and 2017. He also received the Ultra-Broadband Nanoscale Communication and Networking Laboratory Researcher of the Year Award in 2016. In 2016, he received the University at Buffalo Engineering Leaders in Excellence Award for his excellent leadership skills through scholastic accomplishments. He is a member of the SPIE.